

JOPP-3D: Joint Open Vocabulary Semantic Segmentation on Point Clouds and Panoramas

Sandeep Inuganti^{1,2}, Hideaki Kanayama³, Kanta Shimizu^{3,4}, Mahdi Chamseddine^{1,2}, Soichiro Yokota^{3,4}, Didier Stricker^{1,2}, and Jason Rambach¹

¹ German Research Center for Artificial Intelligence, DFKI, Germany

² RPTU Kaiserslautern, Germany

³ Ricoh Company, Ltd. Japan

⁴ Ricoh International B.V. - Niederlassung Deutschland, Germany

Abstract. Semantic segmentation across visual modalities such as 3D point clouds and panoramic images remains a challenging task, primarily due to the scarcity of annotated data and the limited adaptability of fixed-label models. In this paper, we present JOPP-3D, an open-vocabulary semantic segmentation framework that jointly leverages panoramic and point cloud data to enable language-driven scene understanding. We convert RGB-D panoramic images into their corresponding tangential perspective images and 3D point clouds, then use these modalities to extract and align foundational vision-language features. This allows natural language querying to generate semantic masks on both input modalities. Experimental evaluation on the Stanford-2D-3D-s and ToF-360 datasets demonstrates the capability of JOPP-3D to produce coherent and semantically meaningful segmentations across panoramic and 3D domains. Our proposed method achieves a significant improvement compared to the SOTA in open and closed vocabulary 2D and 3D semantic segmentation.

Keywords: 3D Segmentation · Point Clouds · Open vocabulary

1 Introduction

Semantic understanding of complex real-world environments is a fundamental requirement for autonomous systems and robotics. Traditional semantic segmentation approaches rely heavily on large-scale annotated datasets [8], which are often infeasible to obtain and label in unstructured and dynamically changing domains. Moreover, existing segmentation methods are typically constrained to either 2D images or 3D point clouds and depend on predefined class sets that limit their generalization to new object categories [26, 34]. These limitations hinder the scalability and adaptability of perception systems in open and evolving environments where new objects frequently appear, and exhaustive annotation is impractical.

Recent advances in vision-language models (VLMs) have shown the potential of open-vocabulary segmentation, enabling models to recognize and localize arbitrary objects through natural language queries without explicit training

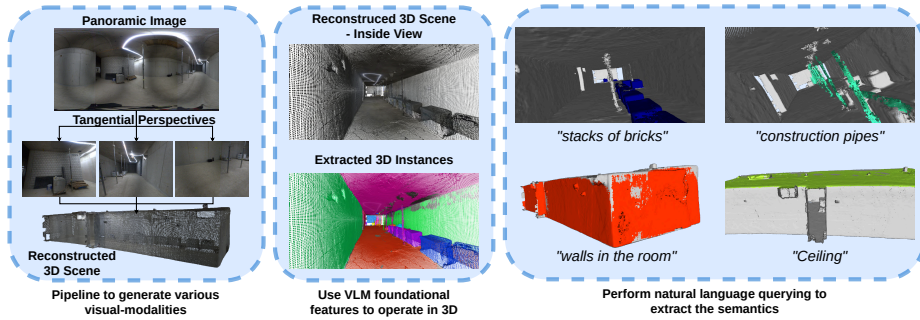


Fig. 1: Joint treatment of panoramas and 3D point clouds in JOPP-3D. Example of zero-shot performance on a construction site scene with varying mask scale.

labels. Foundational works such as CLIP [28] have demonstrated strong cross-modal alignment between visual and textual features, inspiring open-vocabulary extensions to image segmentation tasks [20, 23]. However, most existing works focus exclusively on perspective images and do not generalize well to panoramic imagery or 3D point clouds, both of which are essential for comprehensive spatial understanding. Panoramic images offer complete 360° coverage [7, 49], while 3D point clouds provide geometric fidelity [19, 25]. However, current research has not yet addressed the joint semantic interpretation of these modalities in an open-vocabulary context. Furthermore, aligning 2D panoramic domains and 3D spatial representations remains a major challenge due to geometric distortions, sparse depth estimation, and modality gaps.

To address these challenges, we propose a unified framework for open-vocabulary semantic segmentation of 3D point clouds and panoramic images, leveraging large pre-trained models [18, 28] to achieve label-free and language-driven segmentation. Our approach bridges 2D-3D understanding by constructing 3D point clouds directly from panoramic images and enabling consistent semantic prediction across both modalities. The main contributions of this work are summarized as follows:

- A joint segmentation approach that performs open-vocabulary semantic segmentation on both 3D point clouds and panoramic images using vision-language embeddings.
- An effective pipeline for adapting panoramic inputs to open-vocabulary segmentation by leveraging tangential decomposition, enabling wide-field coverage while maintaining compatibility with vision-language models.
- A 3D to panoramic semantic label propagation method via depth correspondence to enable multi-view-consistent semantic maps.
- Extensive evaluation showing that the proposed framework produces consistent semantic predictions across visual modalities, surpassing the SOTA on both point cloud and panoramic image evaluation metrics.

JOPP-3D is the first approach to tackle the problem of open-vocabulary based semantic segmentation on 3D point clouds and panoramic imagery jointly. We propose two model paradigms: a weakly-supervised and an unsupervised variant that demonstrate the feasibility of achieving open-vocabulary segmentation without labeled data.

2 Related Work

2.1 3D Segmentation

3D scene segmentation aims to assign semantic or instance-level labels to each point in a 3D point cloud, thereby enabling detailed understanding of object geometry and spatial layout in complex environments. The introduction of deep learning revolutionized point cloud processing. PointNet [26] and PointNet++ [27] pioneered direct learning on point sets by aggregating point-wise and local neighborhood features, eliminating the need for voxelization. Transformer-based architectures, including PointTransformer and its variants [5, 39, 40, 48], further enhanced contextual reasoning. Other research trends have explored multimodal and cross-domain 3D segmentation, integrating complementary data such as multi-view images [14, 35] or leveraging self-supervised and contrastive learning for pretraining [13].

Despite these advances, most existing frameworks are constrained by fixed taxonomies and the necessity of large-scale annotated datasets, which are difficult to obtain in unstructured real-world environments. In contrast, open-vocabulary 3D segmentation seeks to overcome these limitations by coupling 3D perception models with vision-language representations [16, 25]. By leveraging pre-trained models such as CLIP [28], these approaches enable segmentation guided by natural language queries, allowing for zero-shot generalization to unseen categories.

2.2 Handling Panoramic Imagery

Unlike conventional perspective images, panoramic or equirectangular images capture the full field of view, making them particularly useful for robotics, autonomous driving, and construction monitoring [17, 36, 43]. However, their inherent geometric distortions, wide spatial coverage, and large variations in object scale pose significant challenges for traditional segmentation networks designed for planar projections. To address these issues, specialized deep learning architectures [11, 33, 46] were proposed, enabling more consistent and geometry-aware feature extraction. Despite these advances, panoramic segmentation methods remain largely limited to supervised training and closed-set class definitions.

On the other hand, foundation models such as SAM [18] and CLIP [28] have strong potential for understanding semantics in perspective images. However, directly applying them to panoramic images is non-trivial due to geometric distortions. To tackle this, there are three feasible approaches: polyhedral projection [30], Cubemap representation [6, 37], and deformable adapter network

(DAN) [49]. Cubemap projection unfolds a 360° panorama onto the six faces of a cube, providing individual views with a 90° field of view (FoV), however this results in artifacts from boundary discontinuities. Meanwhile, DAN from the RGB-only method OPS [49] requires supervised training to provide perspective-based representations for their downstream open-vocabulary segmentation.

In contrast, our method proposes a training-free variant, eliminating the need for learning to model deformations. Furthermore, by incorporating depth information and operating in 3D, our approach produces semantically consistent panoramic segmentation. Our approach uses a tangential decomposition that approximates the sphere using a regular polyhedron and project the panorama onto its F faces. This introduces inter-view overlap, mitigating boundary discontinuities. Prior approaches [9] explored this idea [30], however, the Field of View (FoV) per face is limited to 73.1°, which constrains contextual coverage. To improve this, we use a perspective-projection-based approach, which allows for a wider FoV of 100° per perspective image (more details in Sec 3.1).

2.3 Open-vocabulary scene understanding

VLMs have recently emerged as a powerful paradigm for enabling open-vocabulary and language-guided perception in computer vision. The seminal model, CLIP [28], and the subsequent efforts [15, 21], establish a semantic bridge between images and natural language that generalizes effectively to downstream tasks.

In 2D scene understanding, VLMs have been integrated into open-vocabulary object detection and segmentation [3, 23, 42, 45]. Extending these ideas to 3D data has attracted significant attention. Recent works [10, 25] have explored mapping 3D representations into the same embedding space as pre-trained VLMs to perform open-vocabulary 3D scene understanding. These methods typically project 3D point features into the feature space learned by CLIP, enabling natural language-based querying and reasoning. Further, to mitigate the noisy representations from per-point embeddings, recent open-vocabulary 3D approaches aggregate vision–language features over class-agnostic instance masks, resulting in more stable embeddings. While prior efforts [32] primarily focus on open-vocabulary 3D instance segmentation using perspective RGB-D image sequences, our work instead targets joint semantic segmentation of panoramic images and reconstructed 3D point clouds. In contrast to instance-centric formulations, we address full scene-level segmentation, enabling recognition of both object instances and large structural elements (e.g., *walls* and *floors*).

In summary, our work builds upon this growing body of research by extending VLM capabilities to both 3D point clouds and panoramic images, aiming to achieve unified, label-free scene understanding across visual modalities.

3 Methodology

Formally, for each scene we are provided with a set of panoramic images $\{\mathbf{I}^p \in \mathbb{R}^{W \times H \times 3}\}$, their depth maps $\{\mathbf{D}^p \in \mathbb{R}^{W \times H}\}$, and camera poses $\{[\mathbf{R}^p, \mathbf{t}^p] \in$

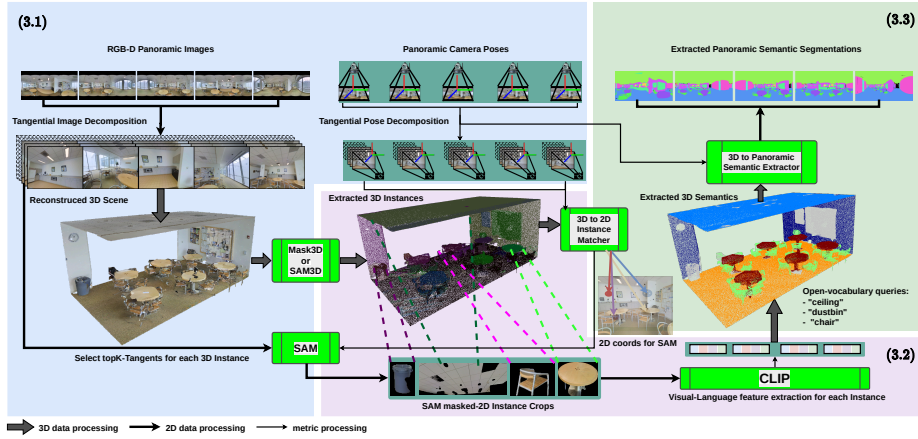


Fig. 2: Methodology: Sec.(3.1) We decompose all the panoramic captures of a scene into their corresponding tangential perspectives and depths. The other outputs of this step are also the tangential poses and the 3D point cloud. Sec.(3.2) We then use these different visual modalities to extract 3D instances [29, 44] of the reconstructed scene and align these instances with CLIP [28] embeddings. Sec.(3.3) In the final step we use open-vocabulary querying to extract the required 3D scene semantics, and further use a depth correspondence-based 3D-to-panoramic semantic extraction method, to obtain the semantic segmentation for each panoramic input.

$SE(3)$. Each panoramic capture of this current scene is then decomposed into a set of F perspectives:

$$\mathcal{F}_{\text{TD}}(\mathbf{I}^p, \mathbf{D}^p, [\mathbf{R}^p, \mathbf{t}^p]) = \{(\mathbf{I}_r, \mathbf{D}_r, [\mathbf{R}_r, \mathbf{t}_r])\}_{r=1}^F \quad (1)$$

where \mathcal{F}_{TD} is our Tangential Decomposition process from which we reconstruct a unified 3D point cloud representation of the scene, $\mathcal{P}^{3\text{D}} = \{\mathbf{p}_i \in \mathbb{R}^3\}_{i=1}^N$ (output of Sec 3.1). Using $\mathcal{P}^{3\text{D}}$ and its corresponding set of tangential decompositions $\{\mathcal{F}_{\text{TD}}(\mathbf{I}^p, \mathbf{D}^p, [\mathbf{R}^p, \mathbf{t}^p])\}$, we extract semantic labels q_i and construct semantic point cloud $\mathcal{S}^{3\text{D}} = \{(\mathbf{p}_i, q_i)\}_{i=1}^N$ in Sec 3.2. Finally in Sec 3.3, the output is a set of dense semantic maps $\{\mathbf{S}^p \in \mathbb{R}^{W \times H}\}$ corresponding to $\mathcal{S}^{3\text{D}}$.

To this end, as shown in Fig. 2, we design a unified framework consisting of three major components, each addressing a key challenge in our problem setting.

3.1 Tangential Decomposition

As shown in Fig. 3, we project the panoramic image \mathbf{I}^p and depth \mathbf{D}^p onto the 20 faces of a regular icosahedron, generating tangential decompositions $\{\mathbf{I}_r\}_{r=1}^{20}$ and $\{\mathbf{D}_r\}_{r=1}^{20}$ corresponding to distinct viewing directions. For each pixel (i_r, j_r) in \mathbf{I}_r and \mathbf{D}_r of size $W \times H$, we compute its normalized camera-space direction

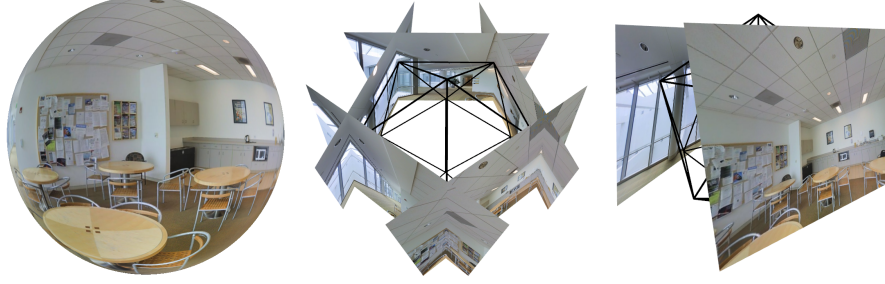


Fig. 3: Representation of a spherical image using tangential decomposition. Left: Original spherical image. Middle: Tangential perspectives mapped onto the faces of an icosahedron. Right: Close-up view of selected tangential perspective images extracted from the spherical image.

by applying the face-specific rotation $\mathbf{R}_{r, \text{local}}$ to the local ray direction:

$$\begin{bmatrix} x_r \\ y_r \\ z_r \end{bmatrix} = \mathbf{R}_{r, \text{local}} \begin{bmatrix} (i_r - W/2)/f \\ (j_r - H/2)/f \\ 1 \end{bmatrix} \quad (2)$$

The focal length f is determined from the horizontal field of view FOV , which we set to 100° in our system to ensure a sufficiently wide coverage per tangent view, exceeding the field of view used in prior work [9], while keeping the perspective projection within a geometrically stable field-of-view range: $f = \frac{W/2}{\tan(FOV/2)}$. This ray in Eq. 2 is converted to spherical angles: $\theta_r = \arctan 2(x_r, z_r)$, $\phi_r = \arctan 2(y_r, \sqrt{x_r^2 + z_r^2})$, and then mapped to equirectangular coordinates (u_r, v_r) :

$$u_r = \frac{\theta_r + \pi}{2\pi} W_e, \quad v_r = \frac{\phi_r + \pi/2}{\pi} H_e \quad (3)$$

Depth from the equirectangular map $\mathbf{D}^p(u_r, v_r)$ is corrected to Z-depth:

$$\mathbf{D}_Z^p(u_r, v_r) = \mathbf{D}^p(u_r, v_r) \cdot \frac{z_r}{\sqrt{x_r^2 + y_r^2 + z_r^2}} \quad (4)$$

Each pixel in the tangential perspective image is mapped to its corresponding location in the panorama: $\mathbf{I}_r(i_r, j_r) = \mathbf{I}^p(u_r, v_r)$, $\mathbf{D}_r(i_r, j_r) = \mathbf{D}_Z^p(u_r, v_r)$. RGB values are sampled using bilinear interpolation for smooth transitions, while depth values use nearest-neighbor interpolation for geometric accuracy. For each tangential face r , we reconstruct its local 3D point cloud and transform all points into the world coordinate system using the camera poses $[\mathbf{R}, \mathbf{t}]^p$:

$$\mathcal{P}_r^{3D, \text{world}} = \mathbf{R}^p \mathbf{D}_Z^p(u_r, v_r) \begin{bmatrix} x_r \\ y_r \\ z_r \end{bmatrix} + \mathbf{t}^p \quad (5)$$

The full 3D point cloud of a panorama is obtained by aggregating all 20 faces. Finally, aggregating all panoramas in the scene and voxelizing yields the global colored 3D reconstruction:

$$\mathcal{P}^{3D} = \text{Voxelize} \left(\bigcup_p \bigcup_{r=1}^{20} \mathcal{P}_r^{3D, \text{world}} \right) \quad (6)$$

3.2 3D Instance Extraction and Semantic Alignment

To enable open-vocabulary semantic reasoning in 3D, we first generate object-agnostic instance proposals from the scene. These proposals serve as the geometric basis for subsequent language-conditioned semantic segmentation and cross-modal alignment. Rather than relying on class-specific supervision, our approach extracts instance-level 3D masks using pre-trained or unsupervised methods, ensuring that the segmentation pipeline remains fully semantic label-free. Specifically, we employ two distinct strategies: (1) **Mask3D**, a supervised model pre-trained on the S3DIS dataset [2], and (2) **SAM3D**, an unsupervised approach capable of generating 3D instance proposals directly from the 2D SAM [18] instance proposals and their corresponding depth maps. We refer the reader to Mask3D [29] and SAM3D [44] for further details on their respective frameworks.

Given the point cloud from our reconstructed scene, $\mathcal{P}^{3D} = \{(x_i, y_i, z_i)\}_{i=1}^N$, 3D instance segmentation provides us with L instance proposals and per-point instance labels $l_i \in \{1, \dots, L\}$. Next, the point sets \mathcal{M}_j for each instance mask are obtained by grouping per instance label:

$$\mathcal{M}_j = \{(x_i, y_i, z_i) \in \mathcal{P}^{3D} \mid l_i = j\}_{j=1}^L \quad (7)$$

Preparing the 3D Instances for Semantic Alignment. The next step is to associate each instance mask \mathcal{M}_j with a corresponding d -dimensional semantic embedding $\mathbf{e}_j^{3D} \in \mathbb{R}^d$ that enables open-vocabulary reasoning. The instance mask plays a crucial role in our framework: due to the wide field of view introduced by the proposed tangential decomposition, each view may contain multiple objects and background regions. By isolating only the pixels belonging to the target instance, the mask prevents semantic contamination from surrounding objects and enables complete and consistent feature aggregation for the object of interest. To achieve this, we start by projecting the 3D points in \mathcal{M}_j into each tangential perspective image \mathbf{I}^t utilizing the tangential pose is given by $[\mathbf{R}^t, \mathbf{t}^t] = [\mathbf{R}_{r, \text{local}} \mathbf{R}^p, \mathbf{t}^p]$. Thus, we obtain the 3D to 2D matched pixel coordinates of instance \mathcal{M}_j in \mathbf{I}^t as

$$\mathbf{M}_j^t(u, v) = \mathbf{K}(\mathbf{R}^t \mathbf{p} + \mathbf{t}^t), \quad \mathbf{p} \in \mathcal{M}_j \quad (8)$$

where \mathbf{K} is the intrinsic of the tangential camera. Now we remove all the matches that are empty and only consider the set of non-empty matches: $\{\mathbf{M}_j^t\}$. We then choose K -tangential images with the highest number of 3D to 2D matched pixel-coordinates by computing $\text{top}_k(K)[\sum_{u_k, v_k} \mathbf{M}_j^t(u, v)]$ for each 3D instance mask \mathcal{M}_j .

2D Instance Segmentation using SAM and Semantic Alignment using CLIP. We have obtained a set of K tangential images $\{\mathbf{I}^t\}_{k=1}^K$ for each \mathcal{M}_j and their corresponding K matched pixel-coordinates $\{\mathbf{M}_j^t(u_k, v_k)\}$. We can now use them as reference points for SAM [18] to compute the instance masks and crops, $\mathbf{S}_{j,k}$, $\mathbf{C}_{j,k}$ in 2D:

$$\mathbf{S}_{j,k}, \mathbf{C}_{j,k} = \text{SAM}(\mathbf{I}_k^t, \mathbf{M}_j^t(u_k, v_k)) \quad (9)$$

producing a consistent set of image crops highlighting the same 3D instance across K tangential views. The instance crops $\mathbf{C}_{j,k}$ are first masked with the instance masks $\mathbf{S}_{j,k}$ and then passed through the CLIP image encoder [28]. This masking of the crops is an important step while encoding instances - we elaborate more on this in Section 4.4. For each instance \mathcal{M}_j , we compute its semantic embedding as the normalized average of its top- K CLIP feature vectors:

$$\mathbf{e}_j^{3D} = \frac{1}{K} \sum_{k=1}^K \frac{\text{CLIP}(\mathbf{S}_{j,k} \odot \mathbf{C}_{j,k})}{\|\text{CLIP}(\mathbf{S}_{j,k} \odot \mathbf{C}_{j,k})\|_2} \quad (10)$$

This aggregated embedding $\mathbf{e}_j^{3D} \in \mathbb{R}^d$ serves as the open-vocabulary semantic descriptor of the 3D instance. With these embeddings, we repeatedly query using natural language for various classes of instances achieving 3D semantic segmentation for the entire scene.

3.3 3D to Panoramic Semantic Extraction

Once the open-vocabulary 3D semantic segmentation has been obtained through language-guided alignment, it is possible to project these semantics back into the panoramic image domain. allowing the model to provide dense, open-vocabulary semantic panoramic image maps, which are more interpretable and useful for downstream visual applications.

Semantic Back-Projection from 3D to Panoramic Domain. Let the 3D semantic point cloud of the current scene, as previously defined be

$$\mathcal{S}^{3D} = \{(\mathbf{p}_i, q_i) \mid (x_i, y_i, z_i) \in \mathcal{P}^{3D}\}_{i=1}^N \quad (11)$$

where $\mathbf{p}_i = (x_i, y_i, z_i) \in \mathbb{R}^3$ denotes the 3D coordinates and $q_i \in \{1, \dots, Q\}$ is the semantic label obtained from the q^{th} open-vocabulary query, in a total of Q different queries, else $q_i = 0$. For each panoramic image \mathbf{I}^p , we have its corresponding camera pose represented by rotation $\mathbf{R}^p \in SO(3)$ and translation $\mathbf{t}^p \in \mathbb{R}^3$. The panoramic depth map $\mathbf{D}^p(u, v)$ provides the depth value of each pixel coordinate (u, v) in the panoramic projection space. We can transform each depth pixel into 3D coordinates in the global point cloud reference frame using:

$$\mathbf{X}^p(u, v) = \mathbf{R}^p \Pi^{-1}(u, v, \mathbf{D}^p(u, v)) + \mathbf{t}^p \quad (12)$$

where $\Pi^{-1}(\cdot)$ denotes the inverse panoramic projection function that maps spherical image coordinates to 3D space. This transformation aligns each panoramic depth point with the coordinate system of the global 3D semantic cloud.

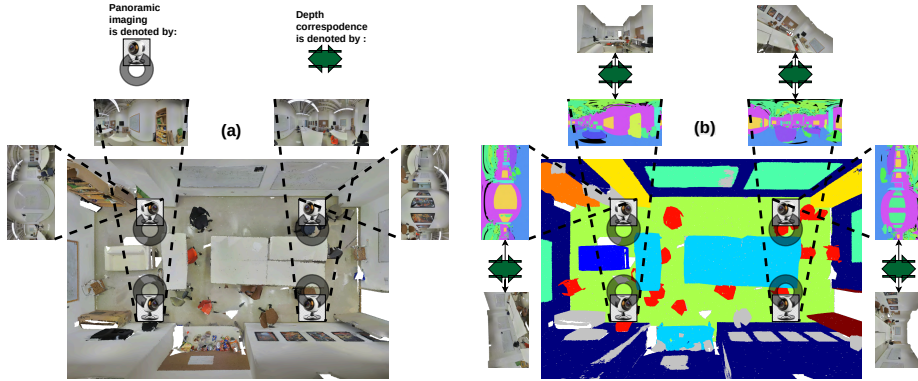


Fig. 4: 3D-to-Panoramic Semantic Extractor. **(a)** Shows the process of panoramic imaging from the top view of a Room. **(b)** We try to emulate the same process on the extracted 3D semantic point cloud by placing the panoramic camera at the same poses. However, after each capture, we transfer the semantic labels of nearby Rooms (scenes) by establishing depth correspondences.

Semantic Association via Nearest-Neighbor Matching. Once the transformed panoramic 3D points $\mathbf{X}^p(u, v)$ are aligned with the 3D semantic point cloud \mathcal{S}^{3D} , we assign to each pixel a semantic label based on its nearest 3D semantic neighbor \mathcal{N} :

$$\mathcal{N}(\mathbf{X}^p(u, v)) = \arg \min_{(x_i, y_i, z_i) \in \mathcal{P}^{3D}} \|\mathbf{X}^p(u, v) - (x_i, y_i, z_i)\|_2 \quad (13)$$

The corresponding panoramic semantic label is then assigned as

$$q^p(u, v) = q_{i^*}, \quad \text{where } i^* = \mathcal{N}(\mathbf{X}^p(u, v)) \quad (14)$$

This process produces a dense semantic map $\mathbf{S}^p = \{q^p(u, v)\}$ in the panoramic domain.

Depth-Correspondence Consistency Across Adjacent Scenes. Direct nearest-neighbor assignment can lead to incomplete semantic projections, particularly near regions such as *doorways* and *corridors*, where panoramic views exhibit large depth discontinuities. To mitigate this, we introduce a depth correspondence strategy that leverages overlapping depth regions between neighboring panoramic scenes, as shown in Fig. 4.

Given two adjacent panoramas \mathbf{I}_1^p and \mathbf{I}_2^p with overlapping depth ranges, we define a local correspondence set:

$$\Omega_{1,2}^p = \{(u, v) \mid |\mathbf{D}_1^p(u, v) - \mathbf{D}_2^p(u', v')| < \delta_d\} \quad (15)$$

where (u', v') denotes the pixel in \mathbf{I}_2^p that projects to approximately the same 3D location as (u, v) in \mathbf{I}_1^p , and δ_d is a small depth threshold that controls the

tolerance of the correspondence. For each missing pixel value in \mathbf{S}_1^p , we propagate the semantic embedding from \mathbf{S}_2^p if a valid correspondence exists:

$$q_1^p(u, v) = \begin{cases} q_2^p(u', v'), & \text{if } (u, v) \in \Omega_{1,2}^p \text{ and } q_1^p(u, v) = 0 \\ q_1^p(u, v), & \text{otherwise} \end{cases} \quad (16)$$

This correspondence-guided refinement ensures semantic continuity across overlapping regions and maintains scene-level consistency in panoramic segmentation. We show the effectiveness of this strategy in section 4.4.

4 Evaluation

In this section, we demonstrate the effectiveness of our proposed open-vocabulary segmentation framework on both the 3D point cloud and panoramic image domains. We evaluate the performance of JOPP-3D on two publicly available datasets that contain both point cloud and panoramic semantic labels. We analyze both quantitative metrics and qualitative visualizations to provide a comprehensive understanding of its capabilities.

Table 1: Point cloud semantic segmentation results on the S3DIS [2] and the ToF-360 [17] datasets. The best performance for each category is shown in **bold**, and the second best is underlined. **s**: supervised, **w**: weakly-supervised, **u**: unsupervised.

(a) Point cloud Segmentation on the S3DIS [2]				
Setting	Method	Supervision	mIoU(%)	mAcc(%)
Closed Vocab	KPConv [34]	s	67.1	72.8
	PointContrast [41]	s	68.1	73.5
	PointTransformer [48]	s	70.4	76.5
	PointTransformerV2 [40]	s	71.6	77.9
	PointTransformerV3 [39]	s	73.4	78.9
	Sonata [38]	s	76.0	81.6
	Concerto [47]	s	77.4	<u>85.0</u>
Open Vocab	OpenMask3D [32]	w	36.7	43.6
	JOPP-3D(u)(ours)	u	59.4	70.1
	JOPP-3D (ours)	w	80.9	87.0

(b) Point cloud Segmentation on the ToF-360 [17]				
Setting	Method	Supervision	mIoU(%)	mAcc(%)
Closed Vocab	PointTransformerV3 [39]	u	18.6	25.1
	SFSS-MMSI [11]	u	<u>23.2</u>	<u>46.3</u>
Open Vocab	JOPP-3D(u) (ours)	u	30.9	47.5

4.1 Datasets

To evaluate the proposed open-vocabulary semantic segmentation framework, we employ two benchmark datasets that provide both panoramic imagery and 3D point clouds with aligned semantic labels: Stanford-2D-3D-s [1] and ToF-360 [17].

These datasets enable a fair assessment of our approach across different scene types, sensor modalities, and annotation styles.

The **Stanford-2D-3D-s** [1] dataset contains high-resolution equirectangular panoramic images paired with registered 3D point clouds, each annotated with pixel-wise and point-wise semantic labels across 13 classes. This dataset serves as a standard benchmark for both panoramic image segmentation and indoor 3D scene understanding. S3DIS [2] is the 3D-only version of this dataset. We evaluate on the Fold-1 of Stanford-2D-3D-s (which is Area-5 of S3DIS) containing panoramic captures covering 68 smaller areas, including *offices*, *hallways*, *conference rooms*.

ToF-360 [17] is a testing-only dataset providing a complementary setup featuring synchronized Time-of-Flight [12] (ToF) depth maps and 360° panoramic RGB images along with corresponding semantic annotations. This dataset consists a total of 4 areas: $2 \times$ *office spaces*, $1 \times$ *hospital*, and $1 \times$ *parking lot*.

Table 2: Panoramic semantic segmentation performance on the Stanford-2D-3D-s [1] and the ToF-360 [17] datasets.

(a) Panoramic Segmentation on Stanford-2D-3D-s [1]					
Setting	Method	Modality	Supervision	mIoU(%)	Open mIoU(%)
Closed Vocab	TangentImg [9]	RGB-D	s	50.6	-
	Trans4PASS+ [46]	RGB	s	53.6	-
	SGAT4PASS [22]	RGB	s	56.4	-
	360BEV [33]	RGB-D	s	56.5	-
	PanoSAMic [4]	RGB-D	s	<u>61.7</u>	-
Open Vocab	OpenMask3D [32]	RGB-D	w	29.8	41.4
	OPS [49]	RGB	w	41.1	42.6
	JOPP-3D(u)(ours)	RGB-D	u	52.8	59.9
	SAM3 [3]	RGB	u	54.2	<u>62.8</u>
	JOPP-3D (ours)	RGB-D	w	70.1	74.6
(b) Panoramic Segmentation on the ToF-360 [17]					
Setting	Method	Modality	Supervision	mIoU(%)	Open mIoU(%)
Closed Vocab	SFSS-MMSI [11]	RGB-D	u	24.9	-
	HoHoNet [31]	RGB-D	u	<u>27.5</u>	-
Open Vocab	JOPP-3D(u) (ours)	RGB-D	u	30.7	47.4

4.2 Experiment Setting

Implementation Details All experiments are conducted on a workstation equipped with an **Intel Xeon CPU @ 3.60 GHz** (12 cores), **64 GB** of RAM, and a single **NVIDIA RTX A6000 GPU** with **48 GB** memory. For panoramic image processing, we generate **20** tangential perspective images of size 640×480 from each panoramic image of size 4096×2048 .

For 3D instance proposals, JOPP-3D receives weak-supervision from a frozen Mask3D [29] checkpoint pre-trained on Areas 1, 2, 3, 4, and 6 of the S3DIS dataset [2]. The unsupervised variant JOPP-3D(u), replaces Mask3D with SAM3D [44]. The original SAM3D implementation has an adjacency-based local and global merging strategy to generate a full 3D instance segmentation of the

given scene. While we follow their global merging, for local merging, we employ a better-suited strategy, taking advantage of our tangential image decomposition (more details provided in the supplementary material).

During open-vocabulary evaluation, we use natural language queries corresponding to each dataset category. In most cases, the query substitute is identical to the original category name. However, for certain ambiguous categories such as “board”, we adopt contextually specific substitutes such as “white board” to provide a clearer semantic ground.

Evaluation Metrics We adopt both 2D and 3D evaluation metrics to assess the performance of our framework. For 2D panoramic semantic segmentation, we report two variants of mean Intersection-over-Union (mIoU): closed-vocabulary mIoU (mIoU) and open-vocabulary mIoU (Open mIoU). We term the standard mIoU as “closed-vocabulary” mIoU because it does not consider semantic similarities between related categories. The Open mIoU, following the evaluation

Table 3: Per-category results on the Stanford-2D-3D-s [1].

<i>Method</i>	<i>mIoU (%)</i>	<i>Beam</i>	<i>Board</i>	<i>Bookcase</i>	<i>Ceiling</i>	<i>Chair</i>	<i>Clutter</i>	<i>Column</i>	<i>Door</i>	<i>Floor</i>	<i>Sofa</i>	<i>Table</i>	<i>Wall</i>	<i>Window</i>
Trans4PASS+ [46]	53.6	0.4	74.4	65.3	<u>84.2</u>	62.9	36.4	16.0	32.8	93.1	44.1	63.7	75.0	46.9
SGAT4PASS [22]	56.4	0.7	74.1	65.9	<u>84.2</u>	64.5	<u>41.2</u>	19.6	52.7	93.1	56.9	58.9	76.4	44.6
360BEV [33]	<u>56.5</u>	0.6	74.6	65.0	84.0	62.4	40.3	18.7	42.2	93.3	53.9	<u>65.9</u>	76.2	58.8
PanoSAMic [4]	<u>61.7</u>	3.3	72.5	<u>68.7</u>	85.8	<u>71.4</u>	39.4	<u>39.7</u>	52.0	96.8	64.2	71.1	<u>79.9</u>	57.1
OPS [49]	41.1	0.0	50.7	44.8	68.8	51.8	8.1	0.0	48.2	71.1	33.6	47.2	55.4	54.5
JOPP-3D(u) (ours)	52.8	<u>14.4</u>	<u>82.4</u>	55.2	66.9	46.0	29.2	19.8	56.0	80.0	<u>69.7</u>	41.1	62.8	52.2
SAM3 [3]	54.2	10.5	72.9	61.0	82.1	64.3	10.8	11.4	<u>59.6</u>	78.9	50.7	51.7	78.2	73.5
JOPP-3D (ours)	70.1	25.8	83.9	71.7	81.9	86.6	45.2	60.2	76.8	<u>95.2</u>	85.9	64.3	81.6	<u>66.8</u>

proposed in [50], leverages semantic relationships from WordNet [24] to consider conceptually similar class predictions (e.g., “sofa” and “chair”) as partial matches. This metric better reflects the behavior of open-vocabulary models operating in real-world settings where class boundaries are linguistically fluid. For 3D semantic segmentation, we report the standard 3D mIoU and mean Accuracy (mAcc).

4.3 Quantitative Results

We evaluate JOPP-3D on both point cloud and panoramic semantic segmentation benchmarks to assess its cross-modal effectiveness. Table 1(a) reports results on the S3DIS Area-5 for 3D semantic segmentation. Compared to strong baselines such as PointTransformerV3 [39], and Sonata [38], our JOPP-3D model achieves a new best performance with **80.9% mIoU** and **87.0% mAcc** while being open-vocabulary without semantic supervision. The consistent performance gains across both 2D and 3D modalities demonstrate the capability of our approach

and its ability to bridge language, geometry, and appearance domains. Table 2(a) presents the quantitative comparison of our proposed approach against recent panoramic semantic segmentation methods on the Stanford-2D-3D-s Fold-1 set.

Among the evaluated baselines, closed-vocabulary methods such as 360BEV [33], and PanoSAMic [4] rely on supervised category-specific training, whereas OPS [49] and our proposed JOPP-3D variants support open-vocabulary inference. The full model JOPP-3D achieves a new state-of-the-art performance: **70.1% mIoU** and **74.6% Open mIoU**, surpassing all prior methods across nearly all categories. Notably, our method improves over others in 9/13 classes in Table 3, with particularly strong gains in *Chair*, *Column*, *Door*, and *Sofa*.

Table 1(b), and Table 2(b) presents results on the ToF-360 evaluation dataset. ToF-360 is a challenging benchmark for zero-shot model evaluation, where once again JOPP-3D(u), our unsupervised variant shows clear improvements.

4.4 Ablation Study

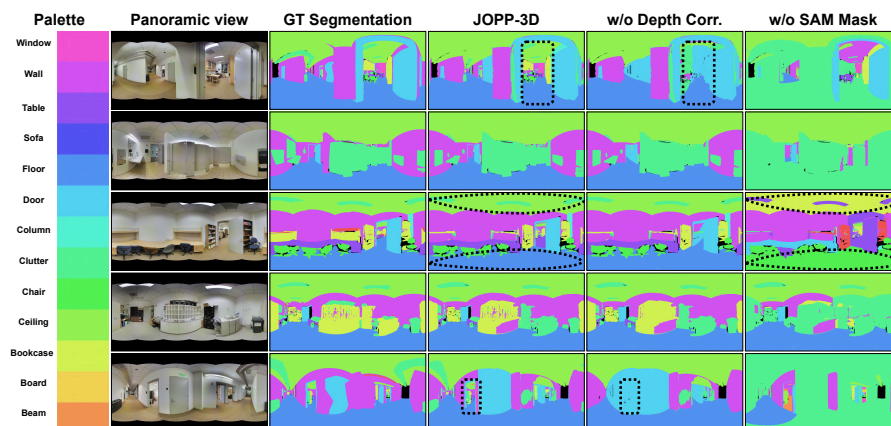


Fig. 5: Qualitative analysis: Each row represents one panoramic capture from a different scene in the Stanford-2D-3D-s [1] dataset. We present the semantic segmentation result from various versions of JOPP-3D. Notable differences are highlighted via dotted curves. In the first and fifth row we can observe why our depth correspondence technique yields segmentations through doors into nearby scenes. In the third row we can see a clear problem of not masking the SAM [18] crops - *floor* and *ceiling* cannot be segmented. Further, querying for *chair* also selects *floor*. Note: The last column has a lot of *clutter* palette. Reason: For *clutter*, we assign all the 3D points that could not be queried using the other 12 classes, and as expected, w/o SAM Mask ablation suffers the worst due to bad CLIP [28] embedding alignment.

To better understand the contributions of each component in our framework, we conduct an ablation study on several variants of our method on the Stanford-2D-3D-s dataset as shown in Table 4. across several variants of our method.

Table 4: Ablation results on the Stanford-2D-3D-s [1]. Ablation studies are done by taking out one component at a time.

<i>Method Variant</i>	<i>Open mIoU (%)</i>	<i>Beam</i>	<i>Board</i>	<i>Bookcase</i>	<i>Ceiling</i>	<i>Chair</i>	<i>Clutter</i>	<i>Column</i>	<i>Door</i>	<i>Floor</i>	<i>Sofa</i>	<i>Table</i>	<i>Wall</i>	<i>Window</i>
w/o SAM Mask	33.6	12.1	56.0	20.2	34.2	52.7	40.9	19.6	32.4	30.2	53.3	30.8	29.0	25.6
w/o Tgt Decomp.	41.4	22.4	55.8	38.4	41.4	60.3	28.2	31.4	40.1	33.1	16.6	43.5	36.8	48.7
JOPP-3D(u)	59.9	22.0	87.6	54.5	68.5	53.1	40.9	28.2	52.5	75.9	74.0	53.5	85.9	60.5
w/o Depth Corr.	67.0	15.1	80.3	62.8	83.2	74.7	54.2	66.0	75.0	90.7	62.6	75.9	79.8	50.2
JOPP-3D	74.6	35.8	86.8	68.2	88.5	85.1	59.0	73.0	82.4	95.2	81.1	81.8	86.6	68.6

Effect of SAM Masking: The variant *w/o SAM Mask* removes the 2D masking step from the instance crops. Without the masking, CLIP embeddings are computed directly on these instance crops, which often contain multiple objects within large instances such as *floor*, *ceiling*, and *walls*. This leads to significant confusion and poor class distinction, resulting in the lowest performance.

Tangential Perspective Decomposition: Using full panoramic images instead of tangentially decomposed perspective views (*w/o Tgt Decomp.*) also degrades performance due to the spherical distortions inherent in panoramic images hindering pertinent CLIP embeddings.

SAM3D vs. Mask3D: Replacing Mask3D with the unsupervised SAM3D yields moderate gains over the previous ablations, demonstrating that high-quality 3D instance proposals are effective for language-guided segmentation.

Depth Correspondence: Finally, removing depth-based correspondence (*w/o Depth Corr.*) adversely affects semantic performance. The lack of precise 3D-to-2D semantic association leads to consistent decrease in performance in all categories compared to our full model, JOPP-3D.

We further support this with qualitative results presented in Fig. 5. Segmentation results on panoramic scenes from the Stanford-2D-3D-s dataset are shown for JOPP-3D as well as for the ablation variants *w/o Depth Corr* and *w/o SAM Mask*. The effect of depth correspondence is clearly visible for areas behind doors. Similarly, the need for masking SAM crops to handle large area classes such as *floor* and *ceiling* is demonstrated. Overall, the ablation study confirms that each component: SAM masking, tangential perspective decomposition, depth correspondence, and reliable 3D proposals – contributes substantially to the final performance.

5 Conclusion

We introduced JOPP-3D, a joint open-vocabulary segmentation framework that unifies point cloud and panoramic semantic understanding without requiring task-specific training. The proposed model pipeline consisting of tangential perspective decomposition, VLM-based semantic alignment, and depth-guided

3D correspondence – effectively bridges panoramic imagery with 3D point clouds. Our ablation study further highlights the importance of each design choice, for achieving fine-grained and spatially consistent segmentation across modalities. Through extensive experiments on the Stanford-2D-3D-s and ToF-360 datasets, we demonstrated that JOPP-3D achieves competitive or superior performance compared to existing panoramic-only or point cloud-only semantic segmentation approaches, while uniquely performing both tasks jointly. Overall, JOPP-3D represents an important step towards scene understanding that connects open-vocabulary reasoning between panoramic and 3D spaces.

A Implementation details for SAM3D

The original SAM3D [44] implementation assumes an input of RGB-D image sequences, where continuous merging is performed by pairing two adjacent frames with sufficient overlap. In contrast, our input consists of discretely captured panoramic RGB-D images, which do not guarantee strong overlap between any two panoramas. To address this, we treat all tangential perspectives generated from a single panorama as an adjacent group and perform sequential merging within this group. We refer to this process as local merging, while merging across panoramas is referred to as global merging.

Both local and global merging follow an overlap-based criterion: two instance masks are merged if their intersection-over-union (IoU) exceeds a predefined threshold. As merged instances grow larger, a higher threshold is required to maintain proper instance separation. In our experiments, we set a relatively low threshold for local merging (0.2) to allow fine-grained merging within a panorama, and a higher threshold for global merging (0.2 – 0.4) to avoid over-merging across panoramas. In contrast, the original SAM3D continuously merges adjacent frames using the same IoU threshold regardless of the merging stage (see Fig. A.1).

B Additional qualitative analysis

A key challenge during the evaluation of JOPP-3D arises from a dataset’s reliance on generic labels due to limitations in annotating capacity. For example, in the Stanford-2D-3D-s [1] dataset, a large variety of semantically meaningful objects – including wall decorations (e.g. clocks, posters), dustbins, and other small furniture are all collapsed into a single “clutter” category. This poses a disadvantage for an open-vocabulary approach such as JOPP-3D, whose strength lies in retrieving semantically coherent concepts using natural-language queries. In contrast, fully supervised methods can simply be trained to deal with “clutter” from large quantities of annotated examples, without having to distinguish the underlying object types.

To better highlight this limitation of the dataset and the advantage of open-vocabulary retrieval, we present additional qualitative results where we directly query fine-grained object categories inside 3D scenes. As shown in Fig. B.1, these concepts can be reliably retrieved using our language-guided 3D semantic

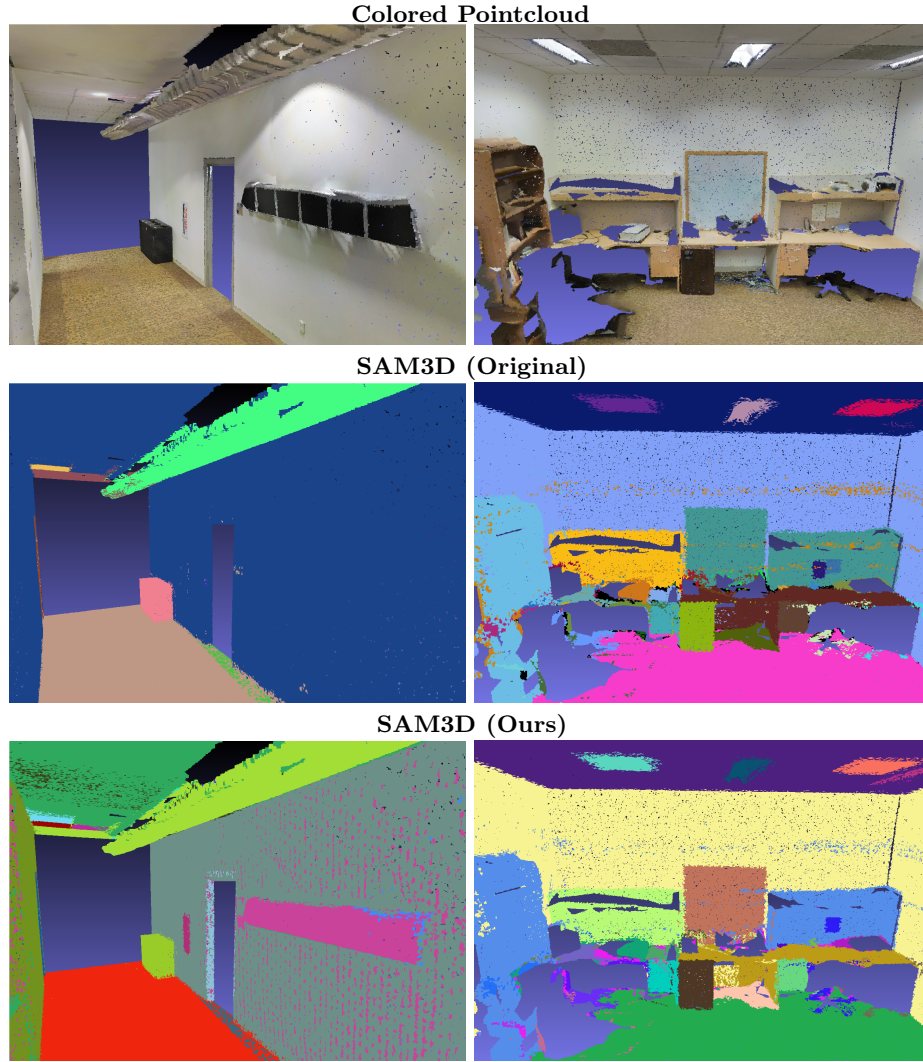


Fig. A.1: Instance segmentation comparison across two different scenes. Rows: Top shows the colored point cloud input; middle shows results from the original SAM3D; bottom shows results from our improved SAM3D with tangent-decomposition-based local and global merging. Columns: Left column corresponds to a hallway scene, and right column to an office scene. In the hallway scene, the original SAM3D merges the ceiling and wall into a single instance, whereas our method achieves clear separation. In the office scene, the original SAM3D merges the whiteboard and desk, while our approach successfully distinguishes them as separate instances.

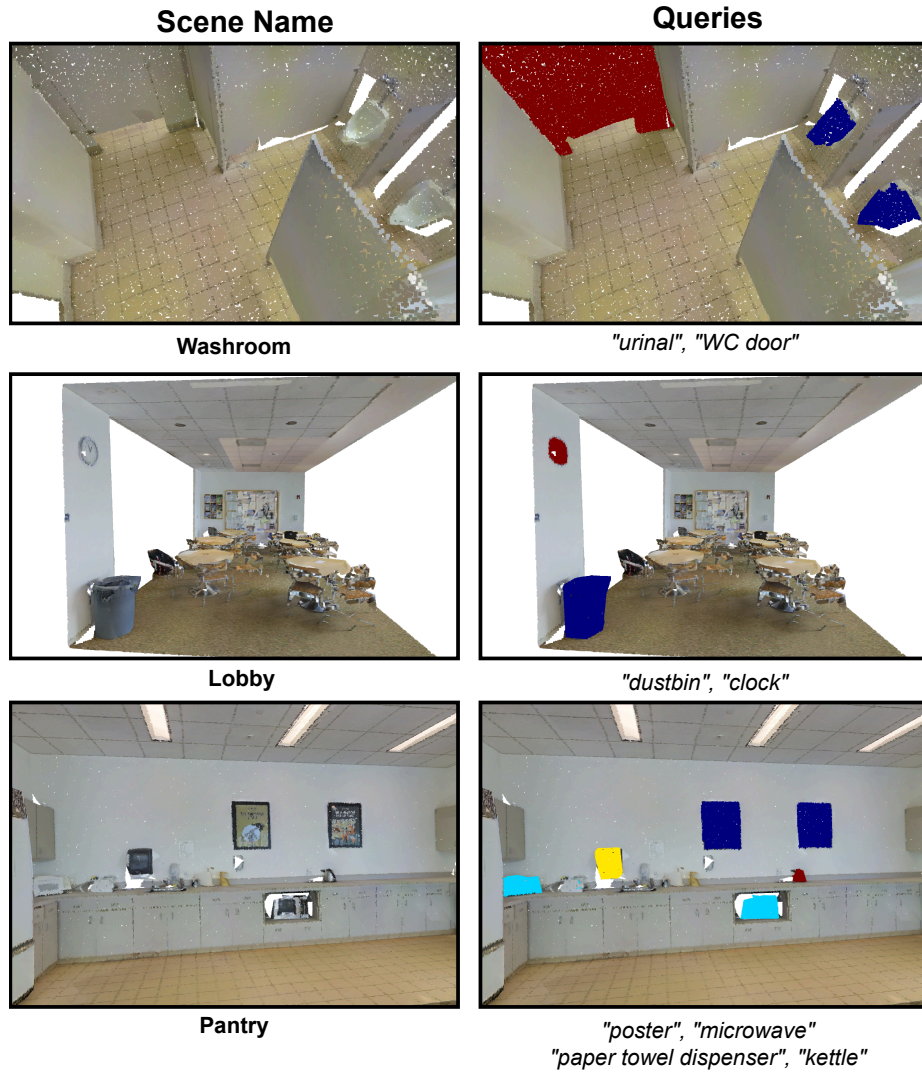


Fig. B.1: First Column: Various 3D scenes, Second Column: The corresponding semantic masks from queries. These objects were marked under “clutter” category in ground-truth semantic annotations, however, JOPP-3D can easily retrieve them.

alignment mechanism, even though all of these items are collapsed into the same clutter label in the ground-truth annotations. While this limits our quantitative scores under the dataset’s closed-set metric, it emphasizes the practical utility of JOPP-3D in real-world environments where semantically rich understanding is required beyond fixed label vocabularies.

C Computational Efficiency

Quantifying computational efficiency for JOPP-3D presents a unique scenario, as our method is entirely training-free. In contrast, most baselines in both panoramic and 3D semantic segmentation require supervised training on large-scale datasets using substantial GPU resources. Nevertheless, following standard compute reporting guidelines, we provide an approximate analysis of inference-time compute usage and efficiency.

The majority of JOPP-3D’s compute cost arises from two inference components: (1) our language-guided semantic alignment pipeline, and (2) the depth-correspondence mechanism used for consistent 3D-to-panoramic semantic transfer. Per panoramic capture of 4096×2048 pixels, our full pipeline averages around 4.8 minutes / image. For a single query, we require roughly 1.7 seconds to retrieve the corresponding semantic masks in the 3D domain. All experiments were performed on a single workstation equipped with an Intel Xeon 12-core CPU with 64 GB RAM and a single NVIDIA RTX A6000 GPU with 48 GB memory.

Although compute-efficiency comparisons are not directly applicable to training-free methods, we contextualize our results against the open-vocabulary baseline, Open Panoramic Segmentation [49], which obtains 41.1 mIoU. JOPP-3D achieves 70.1 mIoU – an improvement of more than 70%. When normalizing compute relative to performance gain, we achieve \approx **0.54 GPU+CPU hours per percentage point**. This relatively low cost highlights the computational efficiency of JOPP-3D, especially given its training-free nature and its ability to jointly perform open-vocabulary segmentation in both panoramic and 3D domains.

References

1. Armeni, I., Sax, A., Zamir, A.R., Savarese, S.: Joint 2D-3D-Semantic Data for Indoor Scene Understanding. ArXiv e-prints (Feb 2017)
2. Armeni, I., Sener, O., Zamir, A.R., Jiang, H., Brilakis, I., Fischer, M., Savarese, S.: 3d semantic parsing of large-scale indoor spaces. In: Proceedings of the IEEE conference on computer vision and pattern recognition. pp. 1534–1543 (2016)
3. Carion, N., Gustafson, L., Hu, Y.T., Debnath, S., Hu, R., Suris, D., Ryali, C., Alwala, K.V., Khedr, H., Huang, A., Lei, J., Ma, T., Guo, B., Kalla, A., Marks, M., Greer, J., Wang, M., Sun, P., Rädle, R., Afouras, T., Mavroudi, E., Xu, K., Wu, T.H., Zhou, Y., Momeni, L., Hazra, R., Ding, S., Vaze, S., Porcher, F., Li, F., Li, S., Kamath, A., Cheng, H.K., Dollár, P., Ravi, N., Saenko, K., Zhang, P., Feichtenhofer, C.: Sam 3: Segment anything with concepts (2025), <https://arxiv.org/abs/2511.16719>
4. Chamseddine, M., Stricker, D., Rambach, J.: Panosamic: Panoramic image segmentation from sam feature encoding and dual view fusion (2026), <https://arxiv.org/abs/2601.07447>

5. Chang, C.P., Wang, S., Pagani, A., Stricker, D.: Mikasa: Multi-key-anchor & scene-aware transformer for 3d visual grounding. In: Proceedings of the IEEE/CVF Conference on Computer Vision and Pattern Recognition. pp. 14131–14140 (2024)
6. Cheng, H.T., Chao, C.H., Dong, J.D., Wen, H.K., Liu, T.L., Sun, M.: Cube padding for weakly-supervised saliency prediction in 360 videos. In: Proceedings of the IEEE Conference on Computer Vision and Pattern Recognition. pp. 1420–1429 (2018)
7. Coors, B., Condurache, A.P., Geiger, A.: Spherenet: Learning spherical representations for detection and classification in omnidirectional images. In: Proceedings of the European conference on computer vision (ECCV). pp. 518–533 (2018)
8. Cordts, M., Omran, M., Ramos, S., Rehfeld, T., Enzweiler, M., Benenson, R., Franke, U., Roth, S., Schiele, B.: The cityscapes dataset for semantic urban scene understanding. In: Proceedings of the IEEE conference on computer vision and pattern recognition. pp. 3213–3223 (2016)
9. Eder, M., Shvets, M., Lim, J., Frahm, J.M.: Tangent images for mitigating spherical distortion. In: Proceedings of the IEEE/CVF Conference on Computer Vision and Pattern Recognition (CVPR) (June 2020)
10. Fu, R., Liu, J., Chen, X., Nie, Y., Xiong, W.: Scene-llm: Extending language model for 3d visual understanding and reasoning. arXiv preprint arXiv:2403.11401 (2024)
11. Guttikonda, S., Rambach, J.R.: Single frame semantic segmentation using multi-modal spherical images. In: WACV. pp. 3210–3219. IEEE (2024)
12. Horaud, R., Hansard, M., Evangelidis, G., M enier, C.: An overview of depth cameras and range scanners based on time-of-flight technologies. *Machine Vision and Applications* **27**(7), 1005–1020 (Jun 2016). <https://doi.org/10.1007/s00138-016-0784-4>, <http://dx.doi.org/10.1007/s00138-016-0784-4>
13. Hou, J., Graham, B., Nie ner, M., Xie, S.: Exploring data-efficient 3d scene understanding with contrastive scene contexts. In: Proceedings of the IEEE/CVF conference on computer vision and pattern recognition. pp. 15587–15597 (2021)
14. Jaritz, M., Gu, J., Su, H.: Multi-view pointnet for 3d scene understanding. In: Proceedings of the IEEE/CVF international conference on computer vision workshops. pp. 0–0 (2019)
15. Jia, C., Yang, Y., Xia, Y., Chen, Y.T., Parekh, Z., Pham, H., Le, Q., Sung, Y.H., Li, Z., Duerig, T.: Scaling up visual and vision-language representation learning with noisy text supervision. In: International conference on machine learning. pp. 4904–4916. PMLR (2021)
16. Jiang, L., Shi, S., Schiele, B.: Open-vocabulary 3d semantic segmentation with foundation models. In: Proceedings of the IEEE/CVF Conference on Computer Vision and Pattern Recognition (CVPR). pp. 21284–21294 (June 2024)
17. Kanayama, H., Chamseddine, M., Guttikonda, S., Okumura, S., Yokota, S., Stricker, D., Rambach, J.: Tof-360-a panoramic time-of-flight rgb-d dataset for single capture indoor semantic 3d reconstruction. In: Proceedings of the Computer Vision and Pattern Recognition Conference. pp. 4442–4451 (2025)
18. Kirillov, A., Mintun, E., Ravi, N., Mao, H., Rolland, C., Gustafson, L., Xiao, T., Whitehead, S., Berg, A.C., Lo, W.Y., et al.: Segment anything. In: Proceedings of the IEEE/CVF International Conference on Computer Vision. pp. 4015–4026 (2023)
19. Kolodiazhnyi, M., Vorontsova, A., Konushin, A., Rukhovich, D.: Oneformer3d: One transformer for unified point cloud segmentation. In: Proceedings of the IEEE/CVF Conference on Computer Vision and Pattern Recognition. pp. 20943–20953 (2024)
20. Li, B., Weinberger, K.Q., Belongie, S., Koltun, V., Ranftl, R.: Language-driven semantic segmentation. In: International Conference on Learning Representations (2022), <https://openreview.net/forum?id=RriDjddCLN>

21. Li, J., Li, D., Xiong, C., Hoi, S.: Blip: Bootstrapping language-image pre-training for unified vision-language understanding and generation. In: International conference on machine learning. pp. 12888–12900. PMLR (2022)
22. Li, X., Wu, T., Qi, Z., Wang, G., Shan, Y., Li, X.: Sgat4pass: Spherical geometry-aware transformer for panoramic semantic segmentation. arXiv preprint arXiv:2306.03403 (2023)
23. Lüddecke, T., Ecker, A.: Image segmentation using text and image prompts. In: Proceedings of the IEEE/CVF conference on computer vision and pattern recognition. pp. 7086–7096 (2022)
24. Miller, G.A.: Wordnet: a lexical database for english. *Commun. ACM* **38**(11), 39–41 (Nov 1995). <https://doi.org/10.1145/219717.219748>, <https://doi.org/10.1145/219717.219748>
25. Peng, S., Genova, K., Jiang, C., Tagliasacchi, A., Pollefeys, M., Funkhouser, T., et al.: Openscene: 3d scene understanding with open vocabularies. In: Proceedings of the IEEE/CVF conference on computer vision and pattern recognition. pp. 815–824 (2023)
26. Qi, C.R., Su, H., Mo, K., Guibas, L.J.: Pointnet: Deep learning on point sets for 3d classification and segmentation. In: Proceedings of the IEEE conference on computer vision and pattern recognition. pp. 652–660 (2017)
27. Qi, C.R., Yi, L., Su, H., Guibas, L.J.: Pointnet++: Deep hierarchical feature learning on point sets in a metric space. *Advances in neural information processing systems* **30** (2017)
28. Radford, A., Kim, J.W., Hallacy, C., Ramesh, A., Goh, G., Agarwal, S., Sastry, G., Askell, A., Mishkin, P., Clark, J., et al.: Learning transferable visual models from natural language supervision. In: International conference on machine learning. pp. 8748–8763. PmLR (2021)
29. Schult, J., Engelmann, F., Hermans, A., Litany, O., Tang, S., Leibe, B.: Mask3d: Mask transformer for 3d semantic instance segmentation. In: 2023 IEEE International Conference on Robotics and Automation (ICRA). pp. 8216–8223. IEEE (2023)
30. Snyder, J.P.: An equal-area map projection for polyhedral globes. *Cartographica: The International Journal for Geographic Information and Geovisualization* **29**, 10–21 (1992), <https://api.semanticscholar.org/CorpusID:122318262>
31. Sun, C., Sun, M., Chen, H.T.: Hohonet: 360 indoor holistic understanding with latent horizontal features. In: Proceedings of the IEEE/CVF Conference on Computer Vision and Pattern Recognition. pp. 2573–2582 (2021)
32. Takmaz, A., Fedele, E., Sumner, R.W., Pollefeys, M., Tombari, F., Engelmann, F.: OpenMask3D: Open-Vocabulary 3D Instance Segmentation. In: Advances in Neural Information Processing Systems (NeurIPS) (2023)
33. Teng, Z., Zhang, J., Yang, K., Peng, K., Shi, H., Reiß, S., Cao, K., Stiefelhagen, R.: 360bev: Panoramic semantic mapping for indoor bird’s-eye view. In: Proceedings of the IEEE/CVF Winter Conference on Applications of Computer Vision. pp. 373–382 (2024)
34. Thomas, H., Qi, C.R., Deschaud, J.E., Marcotegui, B., Goulette, F., Guibas, L.J.: Kpconv: Flexible and deformable convolution for point clouds. In: Proceedings of the IEEE/CVF international conference on computer vision. pp. 6411–6420 (2019)
35. Wang, S., Zhang, S., Millerdurai, C., Westermann, R., Stricker, D., Pagani, A.: Inpaint360gs: Efficient object-aware 3d inpainting via gaussian splatting for 360° scenes. In: Proceedings of the IEEE/CVF Winter Conference on Applications of Computer Vision (WACV). IEEE (2026), accepted for publication

36. Wen, Y., Zhao, Y., Liu, Y., Jia, F., Wang, Y., Luo, C., Zhang, C., Wang, T., Sun, X., Zhang, X.: Panacea: Panoramic and controllable video generation for autonomous driving. In: Proceedings of the IEEE/CVF Conference on Computer Vision and Pattern Recognition. pp. 6902–6912 (2024)
37. Woo Han, S., Young Suh, D.: A 360-degree panoramic image inpainting network using a cube map. *Computers, Materials & Continua* **66**(1), 213–228 (2020). <https://doi.org/10.32604/cmc.2020.012223>, <http://dx.doi.org/10.32604/cmc.2020.012223>
38. Wu, X., DeTone, D., Frost, D., Shen, T., Xie, C., Yang, N., Engel, J., Newcombe, R., Zhao, H., Straub, J.: Sonata: Self-supervised learning of reliable point representations. In: CVPR (2025)
39. Wu, X., Jiang, L., Wang, P.S., Liu, Z., Liu, X., Qiao, Y., Ouyang, W., He, T., Zhao, H.: Point transformer v3: Simpler faster stronger. In: Proceedings of the IEEE/CVF conference on computer vision and pattern recognition. pp. 4840–4851 (2024)
40. Wu, X., Lao, Y., Jiang, L., Liu, X., Zhao, H.: Point transformer v2: Grouped vector attention and partition-based pooling. *Advances in Neural Information Processing Systems* **35**, 33330–33342 (2022)
41. Xie, S., Gu, J., Guo, D., Qi, C., Guibas, L.J., Litany, O.: Pointcontrast: Unsupervised pre-training for 3d point cloud understanding. In: ECCV (2020)
42. Xu, M., Zhang, Z., Wei, F., Hu, H., Bai, X.: Side adapter network for open-vocabulary semantic segmentation. In: Proceedings of the IEEE/CVF conference on computer vision and pattern recognition. pp. 2945–2954 (2023)
43. Yang, K., Hu, X., Chen, H., Xiang, K., Wang, K., Stiefelhagen, R.: Ds-pass: Detail-sensitive panoramic annular semantic segmentation through swaftnet for surrounding sensing. In: 2020 IEEE Intelligent Vehicles Symposium (IV). pp. 457–464. IEEE (2020)
44. Yang, Y., Wu, X., He, T., Zhao, H., Liu, X.: Sam3d: Segment anything in 3d scenes. arXiv preprint arXiv:2306.03908 (2023)
45. Zhang, H., Li, F., Zou, X., Liu, S., Li, C., Yang, J., Zhang, L.: A simple framework for open-vocabulary segmentation and detection. In: Proceedings of the IEEE/CVF International Conference on Computer Vision. pp. 1020–1031 (2023)
46. Zhang, J., Yang, K., Shi, H., Reiß, S., Peng, K., Ma, C., Fu, H., Torr, P.H., Wang, K., Stiefelhagen, R.: Behind every domain there is a shift: Adapting distortion-aware vision transformers for panoramic semantic segmentation. *IEEE Transactions on Pattern Analysis and Machine Intelligence* **46**(12), 8549–8567 (2024)
47. Zhang, Y., Wu, X., Lao, Y., Wang, C., Tian, Z., Wang, N., Zhao, H.: Concerto: Joint 2d-3d self-supervised learning emerges spatial representations. In: NeurIPS (2025)
48. Zhao, H., Jiang, L., Jia, J., Torr, P.H., Koltun, V.: Point transformer. In: Proceedings of the IEEE/CVF international conference on computer vision. pp. 16259–16268 (2021)
49. Zheng, J., Liu, R., Chen, Y., Peng, K., Wu, C., Yang, K., Zhang, J., Stiefelhagen, R.: Open panoramic segmentation. In: European Conference on Computer Vision. pp. 164–182. Springer (2024)
50. Zhou, H., Qi, L., Shen, T., Huang, H., Yang, X., Li, X., Yang, M.H.: Rethinking evaluation metrics of open-vocabulary segmentation. *IEEE transactions on pattern analysis and machine intelligence* (2025)